Materials and Manufacturing Processes, Vol. 15, No. 6, 853–865, 2000

Diamond Turning and Grinding of Aluminum-Based Metal Matrix Composites

Zhaowei Zhong and Nguyen Phu Hung
School of Mechanical and Production Engineering
Nanyang Technological University
Nanyang Avenue, Singapore 639798

Abstract

This paper reports research results obtained from diamond turning and grinding of aluminum-based MMCs reinforced with either SiC or Al_2O_3 particles. Both polycrystal diamond (PCD) and single crystal diamond (SCD) tools were used for turning the MMCs at depths of cut ranging from 0 to 1.6 μm. Diamond grinding wheels were used to grind the MMCs at depths of cut from 0.1 to 1 μm. Besides the depth of cut, ductile-mode turning of the reinforcing particles might also be affected by the orientation of the particles. Grinding using a 3,000-grit diamond wheel at depths of cut of 1 and 0.5 μm produced ductile streaks on the Al_2O_3 particles and the SiC particles, respectively. There was almost no subsurface damage except rare cracked particles. At the same depth of cut, the surfaces ground with the diamond grinding wheel revealed more ductile streaks on the reinforcement ceramic particles than those obtained from SCD turning.

1.0 Introduction

Aluminum-based metal matrix composites (MMCs) reinforced with ceramic particles are known as advanced materials for their good damping properties, high specific strength, and high wear resistance. They are increasingly used in astronautic, automobile, sporting goods and military industries.

Despite such advantages, full implementation of MMCs is cost-prohibitive. This is partially due to the materials' poor machinability. Although near-net-shape MMC components can be produced, final finishing is still needed for the designed final dimensions and required surface finish. A study on machining high performance MMCs, therefore, becomes important especially where mass production is involved.

Copyright ©2000 by Marcel Dekker, Inc.
www.dekker.com

Sensitive cost and fabrication challenges including machining must be overcome for successful application of these composites. The surface finish and surface integrity are important for surface sensitive parts subjected to fatigue or creep. Subsurface damage due to machining of MMCs results from conventional and unconventional processes such as turning, drilling, milling, electrical discharge machining, abrasive jet machining, and laser machining (1-3). Therefore, finishing processes such as grinding and abrasive blasting are utilized to marginally improve the surface integrity of machined MMCs (4-7).

Grinding is performed to obtain a good surface finish, in order to achieve high dimensional accuracy, as well as to remove damaged layers. It was reported that MMCs could be ground with an electroplated diamond wheel (15). 2618/Al_2O_3/10, 20p (10, 20 vol.% Al_2O_3) work-pieces were ground using grinding wheels having SiC in a vitrified matrix and diamond in a resin-bonded matrix (4). Rough grinding with a SiC wheel followed by fine grinding with a fine-grit diamond wheel was recommended, because SiC grains are harder than Al_2O_3 reinforcing particles and much less expensive than diamond grains.

On the other hand, diamond turning may be an alternative to grinding for producing precision MMC components, if cost is not a primary concern. Single crystal diamond tools were used to machine aluminum alloy composites reinforced with 15, 20 or 25 vol.% SiC whiskers (16). The surface finish, Ra, was a function of

1. Relative orientation between the tool rake face and fiber orientation,
2. Cutting speed, and
3. Feed rate. Strong bonding between the matrix and whiskers improved the surface finish. Such strong bonding prevented a whisker from being debonded, or twisted, or pulled out from the matrix during machining.

Meanwhile, research on grinding silicon and germanium revealed that ductile chips could be obtained by properly controlling the depth of cut (17). When a material was machined on such a fine scale that satisfied ductile-mode conditions, the chip was removed in a ductile manner despite the brittle nature of the material. A model for the critical depth associated with ductile-mode machining has been proposed (18).

$$d_C = b\left(\frac{E}{H}\right)\left(\frac{K_C}{H}\right)^2 \quad (1)$$

In equation (1) d_C is critical depth of machining, E is Young's modulus, K_C is critical surface fracture toughness, H is material hardness, and b is a factor that depends on geometry and process conditions. Further investigation showed that there was a dramatic change of d_C when water or alcohol was used as the grinding fluid.

There was evidence of plastic flow with Al_2O_3, Si_3N_4, and SiC along grinding streaks, and a model based on the combination of two theories was proposed (19)

1. The brittle material softened by the high temperature at the cutting point becomes plastically deformable.
2. The Hertzian surface pressure of two bodies in contact with each other

produces stresses and deformations that cause micro-cracks, which lead to the break down of the grains, causing brittle material erosion.

The concept of ductile-mode machining has led to many innovative applications for machining brittle materials, such as Al_2O_3 and SiC. However, reports on ductile-mode machining of aluminum-based MMCs reinforced with ceramic particles are still very scarce. Machine-induced subsurface damage could cause serious consequences (8-14). Therefore, further studies on ductile-mode machining of the materials to obtain damage free surfaces are required for the application of the materials. This paper reports research results obtained from diamond turning and grinding of aluminum-based MMCs reinforced with either SiC or Al_2O_3 particles.

2.0 Experiments

The details of the tested MMC specimens 6061/Al_2O_3/20p (20 vol.% Al_2O_3), 2618/Al_2O_3/20p (20 vol.% Al_2O_3), A359/SiC/10p-T6 (10 vol.% SiC), and A359/SiC/20p-T6 (20 vol.% SiC) are shown in Table 1. The MMCs are cast aluminum alloys reinforced with Al_2O_3 or SiC particles. Some of the as-cast samples were hot-isostatically pressed and/or aged to enhance the matrix properties.

Table 2 shows the details of the turning and grinding conditions, the diamond cutting tools and the grinding wheel used. The crystalline orientation of the diamond cutting tools was measured using an x-ray diffractometer (Philips X'Pert-MPD). The diamond cutting-edge radius (tool edge sharpness) was measured on an atomic force microscope (AFM, Digital Instruments Nanoscope IIIa).

Short coupons of MMC samples were mounted on a precision fixture using melted wax (T_m = 80°C) to avoid the undesirable effects of mechanical clamping. Continuous facing of short MMC coupons was performed on an ultra-precision machine (Precitech Optimum 2800) that had 8.6 nm feedback resolution. Both polycrystal diamond (PCD) and single crystal diamond (SCD) turning tools were used for the facing operations. All samples were rough faced with a PCD tool at 5 µm, then five passes at 1 µm depth of cut. They were then faced using two passes with a new SCD tool at 1 µm, three passes at 0.2 µm, then three passes at the desired depth of cut. All feed rates were normalized at 2% of tool nose radii. The samples were finally machined at constant depths of cut in the range 0 - 1.6 µm. The cutting speed was 10 - 200 m min^{-1}. Compressed air was used to blow chips away from the machined surface.

Grinding experiments were conducted on an Okamoto PSG-64DX grinding machine. A resin-bonded PCD grinding wheel was used to grind the MMC specimens. The grit size was 3,000 (5 µm average grain size). Depths of cut were 0.1, 0.2, 0.5 and 1 µm, feed rate 20.8 m min^{-1}, cross feed 1 mm. The grinding speed used was 1,100 m min^{-1} (1,000 rpm). The diamond grinding wheel was trued by using a braked truing device (BC-1143) immediately after mounting. Dressing was carried out at the beginning

Table 1. Details of the MMC Specimens Used for the Experiments

Material	A359/SiC/10p-T6 (for Turning & Grinding)	$6061/Al_2O_3/20p$ (for Turning)	$2618/Al_2O_3/10, 20p$ (for Grinding)
Matrix	A359 aluminum alloy: 8.96 wt.% Si, 0.18 Fe, 0.53 Mg, balance Al	6061 aluminum alloy (Al, 0.72 wt.% Si, 0.27 Cu, 0.90 Mg)	2618 aluminum alloy
Rein-forcement	10 vol.% SiC particulate, mean 13 μm, aspect ratio 1.5:1, 97% particle < 25 μm, 6% < 5 μm	20 vol.% Al_2O_3 particulate, median size: 21 ± 2 μm	10 vol.% Al_2O_3 particulate for 10p, particle size: 9.3 μm. 20 vol.% Al_2O_3 particulate for 20p, particle size: 21 μm.
Process	Pouring temperature: 700-710°C. Hot isostatic pressing by heating at 550°C, isostatically pressed at 150 MPa, oven-cooled to 300°C, then air-cooled. Solution heat treated at 540°C, water quenched, peak aged at 155°C.	Extrusion at 427°C Extrusion ratio: 35 : 1 Extrusion speed: 6.1 m min^{-1}	Extrusion at 420-430°C Extrusion ratio: 20 : 1 Extrusion speed: 3 m min^{-1}

of the grinding for each specimen by using a WA dressing stick of 320 grit for fine grinding.

The surface finish of the as-machined samples was measured with a profilometer (Form Talysurf 120 L) or on the AFM in a direction perpendicular to the machining direction. Surface integrity of the machined surfaces and subsurface damage were assessed using a Cambridge-Leica SEM. The samples were observed/ scanned in the as-machined condition, then after etching in Keller's etchant (190 ml H_2O, 5 ml HNO_3, 3 ml HCl, 2 ml HF) to dissolve the smeared aluminum on the surfaces. Selected samples were sectioned, mounted, hand ground, polished, and then etched to show the microstructure at the subsurface.

3.0 Results and Discussions

Examination using the SEM and AFM showed that surfaces of the samples

Table 2. Turning and Grinding Conditions, Diamond Cutting Tools, and Grinding Wheel Used

Turning conditions	Cutting speed: 10-200 m min^{-1}, depth of cut: 0 - 1.6 μm, feed rate: 2% of tool nose radii.
Grinding conditions	Grinding speed: 1,100 m min^{-1}, depth of cut: 0.1, 0.2, 0.5, and 1 μm, cross feed: 1 mm, feed rate: 20.8 m min^{-1}.
Polycrystal diamond cutting tools	0.5 μm grain size; American Standard Association tool geometry: 0°, 0°, 9°, 5°, 60°, 30°, 0.33 mm; edge sharpness 0.5~0.75 μm.
Single crystal diamond cutting tools	(100) rake plane; American Standard Association tool geometry: ± 5 & 0°, 0°, 5°, 5°, 30°, 0°, 0.03~2.06 mm; edge sharpness 0.02~0.08 μm.
Diamond grinding wheel	3,000 grit, resin bond, diameter 350 mm, width 10 mm.

were smeared with the soft aluminum matrix, which covered most of the broken Al_2O_3 particles when machined with a PCD tool. The rubbing and smearing of a PCD tool were inevitable because the PCD tool edge sharpness was in the range of 0.50-0.75 μm which was comparable to or, in some cases, greater than the depth of cut used.

Ductile mode machining of the hard Al_2O_3 particles was confirmed by examining the machined surfaces and the sectioned subsurfaces. At a depth of cut of 1.6 μm, the Al_2O_3 particles were cut in the brittle mode, and some particles were broken as shown in Figure 1. On the other hand, when depths of cut were 1 μm and below, many Al_2O_3 particles were machined in the ductile mode with no cutting marks as shown in Figure 2, but some were shattered in a brittle fashion as shown in Figure 3. There was almost no subsurface damage as shown in Figure 4, except rare cracked particles as shown in Figure 5.

These results verified the calculated value d_c = 1 μm for Al_2O_3. Shattering of Al_2O_3 particles by a diamond tool was probably due to unfavorable orientation of those Al_2O_3 particles with respect to the cutting tool, or defects in the Al_2O_3 particles. A deeper effective depth of cut was possible due to minute rotation of an Al_2O_3 particle when it was first engaged with the cutting tool. Force-measuring experiments revealed that the cutting forces were in the sub-Newton range. Although small, such cutting forces might be enough to separate and rotate some Al_2O_3 particles from the matrix, thus effectively increasing the depth of cut beyond the critical threshold. Plastic

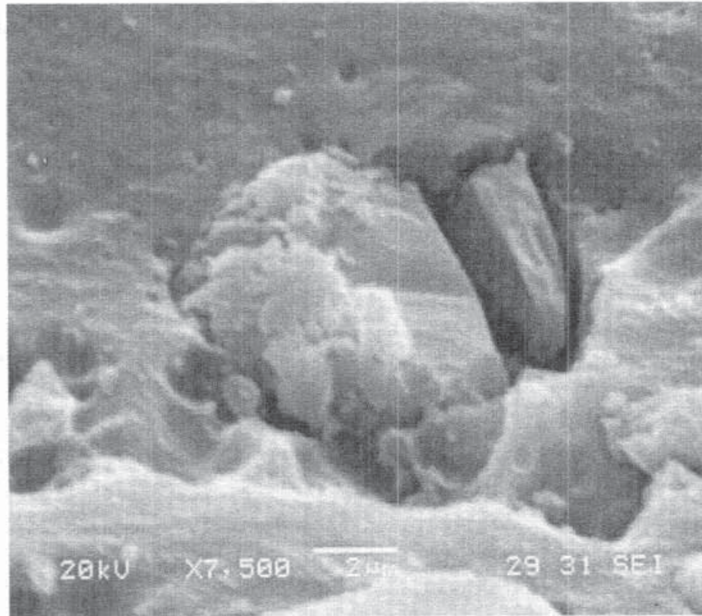

Figure 1: SEM micrograph of turned MMC surface (6061/Al_2O_3/20p, 20 vol.% Al_2O_3). SCD facing then etching with Keller's etchant. Cutting speed: 50 m min^{-1}, depth of cut: 1.6 μm, feed rate: 2% R, R = 0.03 mm. Horizontal cutting direction.

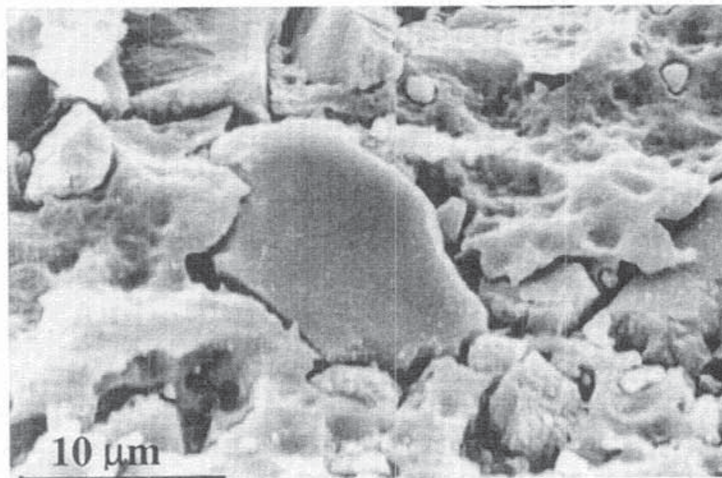

Figure 2: SEM micrograph of turned MMC surface (6061/Al_2O_3/20p, 20 vol.% Al_2O_3). SCD facing then etching with Keller's etchant. Cutting speed: 50 m min^{-1}, depth of cut: 1 μm, feed rate: 2%R, R = 0.03 mm. Horizontal cutting direction.

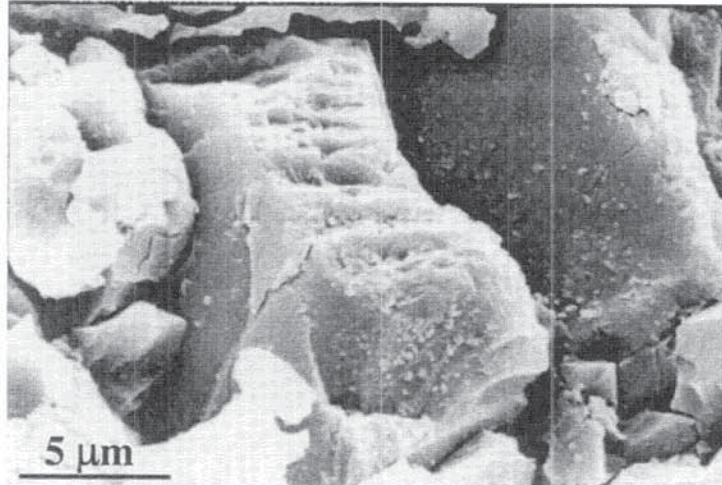

Figure 3: SEM micrograph of turned MMC surface (6061/Al_2O_3/20p, 20 vol.% Al_2O_3). SCD facing then etching with Keller's etchant. Cutting speed: 50 m min^{-1}, depth of cut: 0.4 µm, feed rate: 2% R, R = 0.03 mm. Horizontal cutting direction.

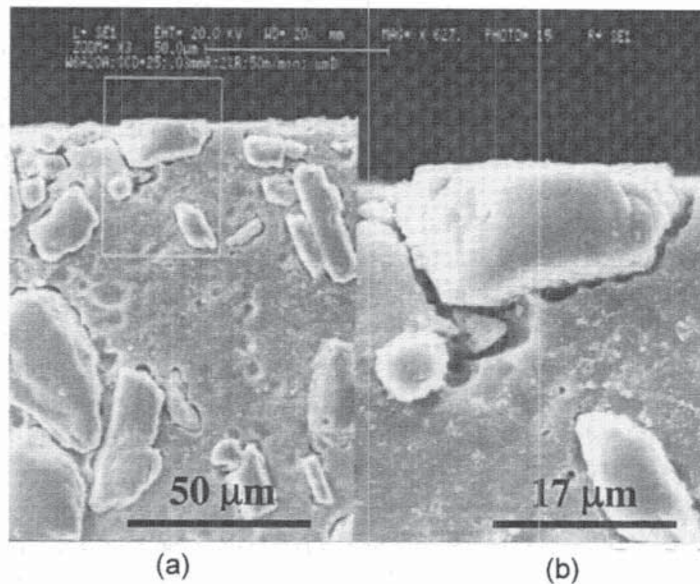

Figure 4: Sub-surface of MMC (6061/Al_2O_3/20p, 20 vol.% Al_2O_3). The image of an Al_2O_3 particle at low magnification in (a) is magnified in (b). SCD facing, cutting speed: 50 m min^{-1}, depth of cut: 1 µm, feed rate: 2% R, R = 0.03 mm.

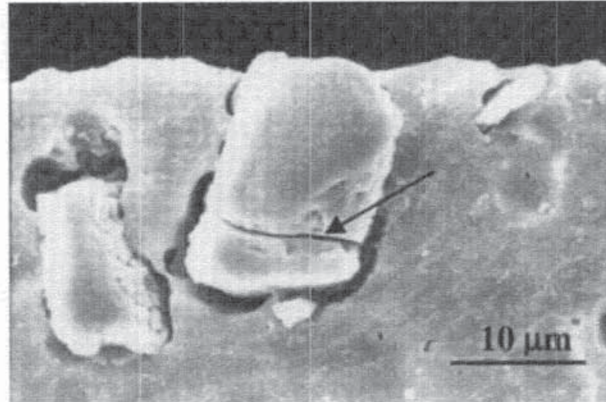

Figure 5: Sub-surface of MMC (6061/Al_2O_3/20p, 20 vol.% Al_2O_3). The arrow points to a very rare crack of an Al_2O_3 particle. SCD facing, cutting speed: 50 m min^{-1}, depth of cut: 1 µm, feed rate: 2% R, R = 0.03 mm.

deformation of the matrix, loosened Al_2O_3 particles from a previous cut, and defects in the particles also contributed to this problem.

The influence of crystal orientation and process conditions was recognized when ductile-mode machining of silicon and germanium was investigated (20-23). The direction of cutting relative to the silicon crystal orientation contributed to the different chip removal mechanisms. The critical depth of cut was 0.14 µm when silicon was machined along the $[2\bar{1}\bar{1}]$ direction, but increased to 0.153 µm for the $[11\bar{2}]$ direction (20). When the (111) silicon wafers were cut, almost 100% ductile mode was seen for all directions at 0.1 µm depth of cut (21). When the (100) germanium was cut with a single crystal diamond tool in distilled water and air, the critical thickness was 0.13 and 0.29 µm, respectively (23).

It was reasonable to assume that ductile-mode machining of Al_2O_3 particles was also affected by the orientation of the particles as well as the physical and mechanical properties. Because it was impractical to control the orientation of all the micro particles, Al_2O_3 particles were randomly distributed in a cast MMC. This explained why many particles, on the same machined surface, were ductile-mode machined but others were machined with micro cleavages or even fractured. Machining at a depth of cut below the critical threshold was only the necessary condition for ductile-mode machining.

The best surface roughness Ra achieved by turning A359/SiC/10p-T6 (10 vol.% SiC) was 17 nm. This was measured on a surface smeared by the aluminum matrix. SEM examination of etched surfaces revealed that the transition between ductile mode and brittle fracture

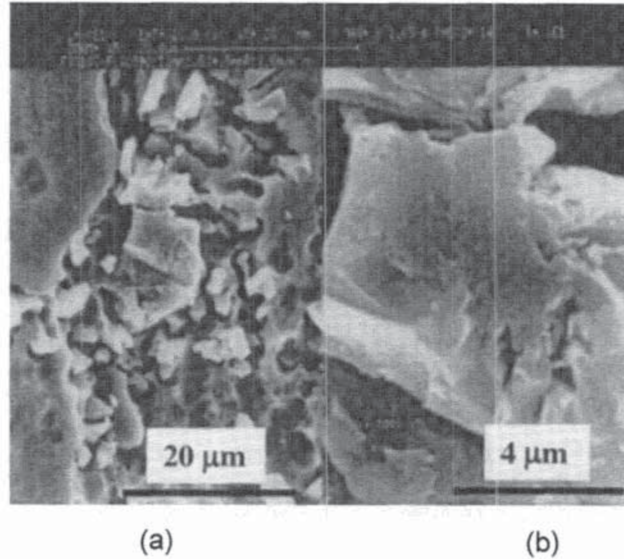

Figure 6: SEM micrograph of turned MMC surface (A359/SiC/10p-T6, 10 vol.% SiC). The image of a SiC particle at low magnification in (a) is magnified in (b). SCD facing then etching with Keller's etchant. Cutting speed: 3.6 m min^{-1}, depth of cut < 0.1 μm, cutter's nose radius R = 0.5 mm. Vertical cutting direction. The surrounding aluminum has been etched.

of SiC particles took place at 0.2 μm depth of cut. Ductile-mode turning of SiC particles was achieved at depths of cut below 0.2 μm. Figure 6 shows cutting marks on a SiC particle.

As shown in Figure 7, grinding of the aluminum composite 2618/Al_2O_3/20p (20 vol.% Al_2O_3) using the fine diamond wheel at 1 μm in-feed (depth of grinding) produced visible ductile streaks on the Al_2O_3 particles. Both the matrix and the Al_2O_3 particles were removed by micro-machining because the ductile grinding marks were clearly seen on the Al_2O_3 particles. There was almost no subsurface damage, as shown in Figure 8.

The diamond wheel also produced A359/SiC/10p-T6 (10 vol.% SiC) surfaces with few SiC-particle-related defects. A very thin smearing layer of aluminum and partially hidden SiC particles were observed on the ground surfaces. When lightly etched with Keller's etchant, the ductile-mode ground surfaces of SiC particles can be seen. As shown in Figure 9, with the experimental depth of cut 0.5 μm, the ductile-mode grinding of a SiC particle was observed.

It was found by comparing the results obtained from the diamond turning and grinding that at the same depths of cut, the surfaces ground with diamond grinding

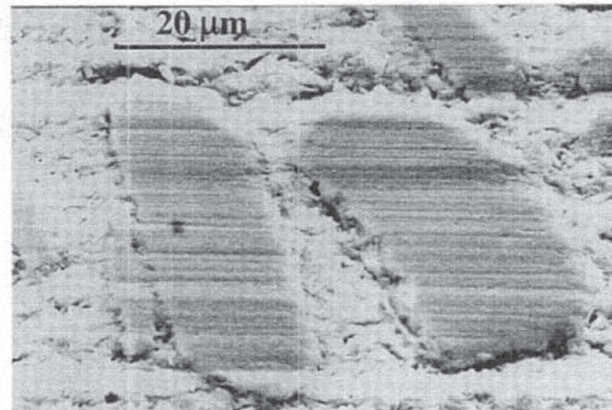

Figure 7: SEM micrograph of ground MMC surface (2618/Al_2O_3/20p, 20 vol.% Al_2O_3). 3,000-grit resin-bond diamond wheel, grinding speed: 1,100 m min^{-1}, depth of cut: 1 μm, crossfeed: 1 mm, feed rate: 20.8 m min^{-1}.

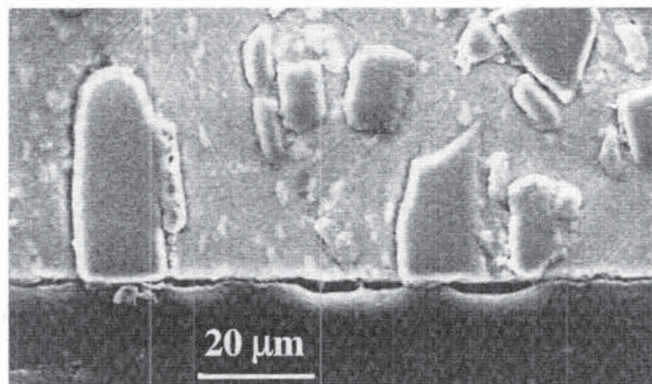

Figure 8: Sub-surface of ground MMC (2618/Al_2O_3/20p, 20 vol.% Al_2O_3). 3,000-grit resin-bond diamond wheel, grinding speed: 1,100 m min^{-1}, depth of cut: 1 μm, crossfeed: 1 mm, feed rate: 20.8 m min^{-1}.

wheels revealed more ductile streaks on the reinforcement Al_2O_3 and SiC particles than those obtained from SCD turning. This is due to the significant difference between turning and grinding mechanisms.

Very unlike turning using a single-point diamond cutter, the grinding used a bonded abrasive wheel which had hundreds of millions of cutting points randomly orientated and irregularly distributed on its working surface. In other

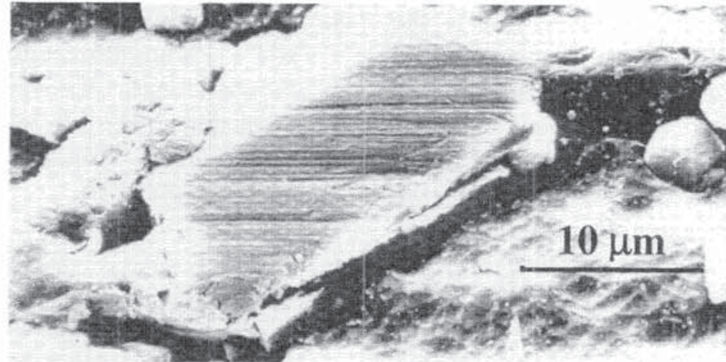

Figure 9: SEM micrograph of ground MMC surface (A359/SiC/10p-T6, 10 vol.% SiC). Diamond wheel, grinding speed: 1,100 m min^{-1}, depth of cut: 0.5 µm, crossfeed: 1 mm, feed rate: 20.8 m min^{-1}.

words, the diamond wheel had hundreds of millions of micro-cutting tools, which interacted with the MMC workpiece. During grinding, at least hundreds of diamond cutting-points simultaneously interacted with the MMC surface. The diamond micro-cutting points were not equally spaced and did not uniformly protrude. Even one diamond grain might have more than one cutting point. The geometry of one cutting point might be different from that of another one.

Therefore, the "critical depth of cut" for grinding has different meaning from that for turning, and might be misleading. 100% ductile-mode mirror grinding of SiC could be achieved by using a non-ultraprecision machine at 1 µm in-feed (depth of grinding) resulting in big mirror surfaces comparable to well polished mirrors (24, 25), although the critical depth of cut for performing ductile-mode machining of SiC was widely regarded as 0.2 - 0.6 µm.

4.0 Summary

Diamond turning and grinding experiments were performed on aluminum-based MMCs reinforced with SiC or Al_2O_3 particles, and conditions for ductile-mode turning for both the matrix and the reinforcement were sought.

The critical depths of cut for performing ductile-mode turning of MMCs reinforced with SiC and Al_2O_3 particles were found to be 0.2 and 1 µm, respectively. At these depths of cut, there was almost no subsurface damage except rare cracked particles. Besides the depth of cut, ductile-mode machining of the reinforcing particles might also be affected by the orientation of the particles.

At the same depths of cut, the surfaces ground with diamond grinding wheels revealed more ductile streaks on the reinforced ceramic particles than those obtained from single-crystal-

diamond turning. This is due to the significant difference between turning and grinding mechanisms. The diamond wheel had hundreds of millions of micro-cutting points that interacted with the MMCs. The "critical depth of cut" for grinding has a different meaning from that for turning. Grinding using a 3,000-grit diamond wheel at depths of cut of 1 and 0.5 μm produced many ductile streaks on the Al_2O_3 particles and the SiC particles, respectively.

5.0 Acknowledgment

The authors would like to thank Duralcan for the composites, Sumitomo and Osaka Diamond for the cutting tools, Mr. T. C. Tan for turning A359/SiC/10p-T6 (10 vol.% SiC), and Mr. J. C. Wong for micro sectioning the turned 6061/ Al_2O_3/20p (20 vol.% Al_2O_3).

6.0 References

1. Hung, N. P., L. J. Yang, and K. W. Leong, Journal of Materials Processing Technology, Vol.44, pp.229-236, (1994).

2. Hung, N. P., S. Jana, L. J. Yang, and C. H. Heng, Proceedings on Machining of Advanced Materials ASME AMD, Los Angeles, Vol.208, pp.87-92, (1995).

3. Hung, N. P., F. Y .C. Boey, K. A. Phua, and H. F. Lee, Journal of Materials Processing Technology, Vol.56, pp.966-977, (1996).

4. Z. W. Zhong, N. P. Hung, N. L. Loh, and T. Sano, Proceedings of the International Conference on Mechanics of Solids and Materials Engineering, Singapore, Vol. A, pp.274-279, (1995).

5. Hung, N. P., Z. W. Zhong, and C. H. Zhong, Proceedings of the Fourth Conference on Composites Engineering, Hawaii, pp.459-460, (1997).

6. Hung, N. P., Z. W. Zhong, and C. H. Zhong, Journal of Materials and Manufacturing Processes, Vol.12, No.6, pp.1075-1091, (1997).

7. Hung, N. P., C. M. Yoong, and B. H. Low, Journal of Materials and Manufacturing Processes, Vol.13, No.1, pp.101-115, (1998).

8. Cronjager, L. and D. Meister, Composite Material Technology, PD., ASME, Vol.37, pp.185-189, (1991).

9. Chen, P., Annals of the CIRP, Vol.41, No. 1, pp.59-62, (1992).

10. Cronjager, L. and D. Meister, Annals of the CIRP, Vol.41, No.1, pp.63-66, (1992).

11. Lane, C., Proceedings of ASM Materials Week, Chicago, pp.3-15, (1992).

12. Monaghan, J. and P. O'Reilly, Journal of Materials Processing Technology, Vol.33, pp.469-480, (1992).

13. Tomac, N. and K. Tonnessen, Annals of the CIRP, Vol.41, No.1, pp.55-58, (1992).

14. Weinert, K. Annals of the CIRP, Vol.42, No.1, pp.95-98, (1993).

15. Konig, W., L. Cronjager, G. Spur, H. K. Tonshoff, M. Vigneau, W. J. Zdeblick, Annals of the CIRP, Vol.39, No.2, pp.673-681, (1990).

16. Yuan, Z. J., L. Geng, and S. Dong, Annals of the CIRP, Vol.42, No.1, pp.107-109, (1993).

17. Blake, P.N. Ductile-Regime Turning of Germanium and Silicon, Ph.D. Thesis, North Carolina State University, Rayleigh, NC., (1988).

18. Bifano, T. G. T. A., Dow, and R. O. Scattergood, Advances in Fabrication and Metrology for Optics and Large Optics, SPE 966, pp.108-115, (1988).

19. Kitajima, K., G. Q. Cai, N. Kumagai, Y. Tanaka, and H.W. Zheng, Annals of CIRP, Vol.41, No.1, pp.367-371, (1992).

20. Leung, T. P., W. B. Lee, and X. M. Lu, Journal of Materials Processing Technology, No.73, pp.28-42, (1998).

21. Shibata, T., S. Fujii, E. Makino, and M. Ikeda, Journal of Precision Engineering, Vol.18, No.2/3, pp.129-137, (1996).

22. Shimada, S., N. Ikawa, T. Inamura, N. Takezawa, H. Ohmori, and T. Sata, Annals of the CIRP, Vol.44, No.1, pp.523-526, (1995).

23. Blackley W. S. and R. O. Scattergood, Journal of Precision Engineering, Vol.13, No.2, pp.95-103, (1991).

24. Zhong, Z. W., Annals of CIRP, Vol.41, No.1, pp.335-338, (1992).

25. Zhong, Z. W. and V. C. Venkatesh, Annals of CIRP, Vol.43, No.1, pp.323-326, (1994).